The Thermal Expansion Characteristics of Stainless Steel Weld Metal

Thermal expansion data are established to help in the proper selection of austenitic stainless steel filler metals to be used for welding dissimilar metal joints

BY J. W. ELMER, D. L. OLSON AND D. K. MATLOCK

ABSTRACT. Thermal expansion coefficients for 28 stainless steel welds of varying composition have been measured. A graphic method of predicting the coefficient of thermal expansion (CTE) for stainless steel welds centered about the DeLong diagram has been prepared from these data. An overall description of the behavior of the CTE as a function of composition was accomplished by supplementing the data with published thermal expansion data of all Fe-Ni-Cr type alloys. Lines of constant expansion were then mapped on the Fe-Ni-Cr ternary diagram and were subsequently transposed to the Schaeffler diagram. Using these diagrams, the CTE for a wide range of ferritic and austenitic alloys can be predicted.

Residual delta ferrite in a stainless steel weld was shown to reduce the CTE of the duplex austenite-ferrite microstructure from that of a ferrite-free microstructure. Results predict the CTE of residual delta ferrite to be 15.0 μm/m/°C over a 20 to 400°C (68 to 752°F) temperature range; in addition, with the Thomas composite theory of thermal expansion, the CTE of any stainless steel weld containing delta ferrite can be calculated. A decrease in specific volume was shown to accompany the transformation of metastable delta ferrite to austenite and sigma phase. This contractive dilation results in a strain of 4.5×10^{-5} per percent ferrite that transforms. It should be emphasized that this strain will, in general, produce stresses that are tensile in nature across a weld joint. Furthermore, the total strain due to the transformation is determined by the initial ferrite content and the time that the joint is held at an elevated temperature.

Introduction

Thermal expansion is a fundamental material property which relates dimensional changes of a material with changes in temperature. A convenient measure of thermal expansion is the mean linear coefficient of thermal expansion (CTE) and is defined as:

$$\alpha_m = \frac{L_2 - L_1}{L_o\,(T_2 - T_1)} = \left(\frac{\Delta L}{L_o}\right)\frac{1}{\Delta T} \qquad (1)$$

where L_1 and L_2 are the specimen lengths at temperatures T_1 and T_2 respectively, L_o is the initial specimen length and α_m is the mean CTE. Fundamentally, the CTE measures the amount of strain, $\Delta L/L_o$, which accompanies a material with a change in temperature, ΔT.

When dissimilar materials are joined and restrained such as in a welding process, changes in temperature will allow stresses as high as the yield stress to develop in the joint. For example, Dalcher et al. (Ref. 1) predicted hoop stresses up to 34 ksi (234 MPa) at the root of a typical dissimilar metal pipe weld due to the CTE mismatch alone. The stresses decay as a function of position away from the interface so that far from the interface the CTE mismatch stresses are zero. The stress distribution is determined by the weld joint design and weldment geometry, while the stress level depends on both the difference in CTE between the weld and base metals and the temperature change from the stress free temperature.

The stress free temperature is the reference temperature at which no CTE stresses exist. Typically, in the as-welded condition, this temperature will be close to the solidus of the weld metal. However, if a postweld heat treatment (PWHT) operation has been used, stress relief may be sufficient to reduce the stresses such that the PWHT temperature will be stress free. If welds of dissimilar metals are used at high operating temperatures, the thermally induced stresses can decay by creep mechanisms to low levels with time. The weldment at the operating temperature will then be essentially stress free. However, stresses will develop when the weld is cooled to room temperature, a particular concern if thermal cycling is frequent.

Selection of the proper filler metal to weld dissimilar metals that minimizes CTE mismatch stresses requires an understanding of the thermal expansion properties of the weld metal. A compilation of published CTE data by Bennett (Ref. 2) for stainless steel welds and base metals was an early attempt to characterize these properties; however, little other information is available on the CTE behavior of weld metal.

Stainless steel filler metals are frequently used to weld austenitic and ferritic steels. Typically, the austenitic stainless steel has a CTE that is 30% to 40% greater than that of a ferritic steel. This CTE mismatch is frequently responsible for problems that occur in these type of joints. One such problem exists with the ferritic Cr-Mo steel to austenitic stainless steel weld transition joint commonly used in power plants (Ref. 3, 4). Numerous service failures resulting in costly downtime have occurred (Ref. 5) in these weld joints, because of fusion line cracking at the ferritic weld interface when Type 310 Cb and other types of stainless steel filler metals were used.

Thermal expansion mismatch has been sited (Ref. 3-6) as one of the major problems with this particular weld. Some degree of success has been obtained in preventing or at least postponing the cracking problem by using ERNiCr-3 nick-

Based on paper presented at the 62nd AWS Annual Convention held in Cleveland, Ohio, during April 5-10, 1981.

J. W. ELMER, D. L. OLSON and D. K. MATLOCK are with the Colorado School of Mines, Golden, Colorado.

el-base filler metal which has a lower CTE than Type 310 Cb stainless steel filler, and has a CTE between that of the two base metals (Ref. 5). Another problem that exists is cracking of weld cladded material (Ref. 7). Austenitic stainless steels are clad on ferritic steels to provide corrosion resistance. Typically these welds cover large surface areas relative to other welding processes, and an understanding of how the CTE varies with dilution would be helpful in selecting proper filler metals.

Before discussing the specific aspects of this study, it is necessary to point out that the CTE of a material is dependent upon the prior thermomechanical processing history and the temperature range over which it is measured. For example, a ferrite-free wrought, stainless steel will have a different CTE than its welded counterpart containing residual delta ferrite, or a 36% nickel-iron alloy (Invar) will have different CTE's depending on the mechanical processing history and the temperature range of interest. It is, therefore, necessary to compare the CTE data for materials that have had the same metallurgical processing history—welds, for example—and whose CTE were measured over identical conditions. Otherwise, the correlations can only be considered approximate. In general, however, these correlations allow engineering trends to be established by means such as the plotting of isoexpansion lines on diagrams as a function of composition, using data acquired from many sources.

Experimental Procedures

Welding and Specimen Preparation

A three step weld alloying procedure, similar to that of Lippold and Savage (Ref. 8), was used to produce welds of desired compositions. This procedure is illustrated in Fig. 1. First, a GMAW process was used to lay a bead on ½ in. thick (12.5 mm) Type 316 stainless steel plate using 1/16 in. (1.6 mm) diameter Type 308, 309, 310, 312, 330 or 410 stainless steel filler metal wire. Welding grade argon-2% oxygen was used as the shielding gas, and the travel speed was varied from 11 ipm (4.65 mm/s) to 28 ipm (11.9 mm/s) to produce several different welds from each filler metal. Next, the weld reinforcement was removed by machining, leaving the base metal intact.

This process left a strip of the GMAW deposited filler metal down the center of the base plate. In the final step, the alloying filler metal and the base metal were melted together using a GTAW pass. Welding grade argon was used as the shielding gas with a 2% thoriated tungsten electrode ground to a 90 deg included angle. The travel speed of this pass was varied from 2.5 ipm (1.07 mm/s) to 3.1 ipm (1.32 mm/s) to provide different amounts of dilution of the GMA deposit with the Type 316 stainless steel base metal.

The different GMAW deposition rates and GTAW dilution rates were used to produce a total of 28 welds of different compositions from the six filler metals. For each filler metal, a series of welds was produced which varied in composition from the base metal to the filler metal. The welding parameters and resulting chemical compositions of the test welds are presented in Table 1. The chemical compositions were measured using emission spectroscopy and interstitial analysis.

In Table 1, the three numbers of the specimen designation refer to the stainless steel filler metal type, and the letters refer to high, medium, low or zero deposition rate (GMAW) and dilution rate (GTAW). For example, 308HL refers to 308 filler metal, high deposition (GMAW), low dilution (GTAW). Note that a high heat input was necessary to produce a weld bead of sufficient size, such that a specimen for dilatometric analysis could be removed. The all-weld-metal dilatometric specimen machined from the center line of the weld bead as shown in Fig. 1C measures 1.5 in. (38 mm) long and 0.15 in. (3.8 mm) in diameter.

Testing Procedure

Thermal expansion measurements were made using a horizontally positioned vitreous silica push rod dilatometer. Dilation curves were recorded as specimen length change versus temperature using an X-Y recorder. NBS standard reference materials SRM 736 (copper) and SRM 737 (tungsten) were used to calibrate the dilatometer. The dilatometer calibration curve was established using the tungsten standard. The copper standard was then tested and from its corrected dilation curve the accuracy of the dilatometer was determined to be ±1.8% error in the mean CTE as determined from 11 data points taken at 25°C (45°F) intervals in the range from 275 to 525°C (527 to 977°F).

All testing was conducted in an argon atmosphere to prevent oxidation of the specimen. The heating rate was controlled at 5.5°C/min (10°F/min) and cooling curves were recorded during a furnace cool at cooling rates less than 5°C/min (9°F/min). The specimen temperature was recorded using a single type K thermocouple that was kept in contact with the center of the specimen during the test. The length change, accurate to 1×10^{-4} in. (2.5×10^{-3} mm), was recorded using an LVDT mounted in a micrometer stage which was separated from the furnace with a water cooled barrier.

The experimental thermal expansion data were corrected to obtain the true dilation curve using the established calibration curve. A microprocessor assembly equipped with a digitizer was used to analyze and fit the true dilation curve to a fourth order polynomial of the form:

$$L = L_o + aT + bT^2 + cT^3 + dT^4 \qquad (2)$$

where specimen length, L, at temperature, T, can be calculated from the original length, L_o, and polynomial coefficients a, b, c, d. Both instantaneous and mean CTE data were calculated from this equation. The polynomial estimation typically fit the actual data with a coefficient of

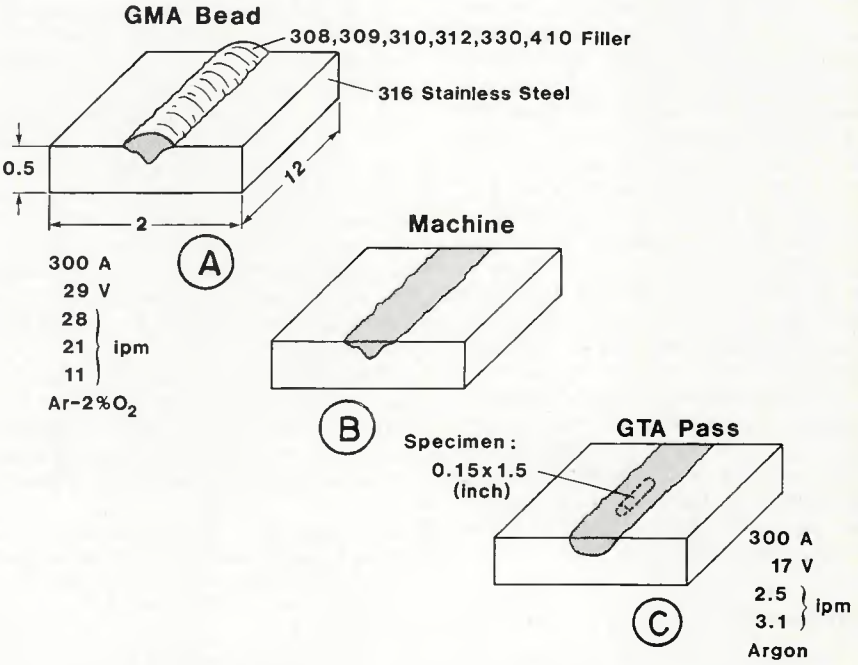

Fig. 1—Three step weld alloying procedure used to produce stainless steel welds

Table 1—Summary of Welding Procedures and Resulting Composition of 28 Stainless Steel Welds

	GMA[a]			GTA[a]			Composition											
Specimen	I	V	S	I	V	S	Cr	Si	Mo	Nb Ti Zr	N	C	Mn	Ni	Cu	Co	S	O
308HΦ	300	28-29	11	N/A	N/A	N/A	19.5	.38	1.27	<.01	.063	.049	1.34	10.4	.31	.17	.017	.054
308HL	300	28-29	11	310	16-17	3.1	18.3	.70	1.68	<.01	.034	.052	1.49	10.3	.09	.21	.005	.015
308HH	300	28-29	11	310	16-17	1.7	17.6	.78	2.00	<.01	.033	.058	1.53	10.3	.08	.20	.006	.013
309HΦ	300	29-30	11	N/A	N/A	N/A	22.6	.39	1.27	<.01	.059	.071	1.53	12.1	.27	.19	.024	.040
309HL	300	29-30	11	310	16-17	3.1	21.0	.44	1.44	<.01	.077	.057	1.72	12.0	.30	.19	.025	.020
309HM	300	29-30	11	310	16-17	2.7	21.5	.41	1.44	<.01	.100	.056	1.80	12.5	.31	.20	.025	.022
309HH	300	29-30	11	310	16-17	2.1	20.0	.36	1.80	<.01	.160	.073	1.33	11.3	.32	.18	.026	.029
309MM	300	29-30	21	310	16-17	2.7	18.7	.40	1.85	<.01	.100	.060	1.37	11.2	.39	.18	.027	.019
309LH	290	29-30	38	310	16-17	2.1	18.5	.42	2.00	<.01	.120	.066	1.25	11.2	.35	.19	.028	.023
310HΦ	290	29-30	11	N/A	N/A	N/A	22.5	.40	1.1	<.01	.075	.082	1.35	15.0	.23	.12	.016	.042
310MM	290	28-29	21	300	17-18	2.7	19.5	.40	2.1	<.01	.075	.063	1.35	12.8	.33	.17	.024	.052
310MH	290	28-29	21	310	17-18	2.1	19.0	.35	2.0	<.01	.078	.065	1.30	12.5	.32	.18	.025	.091
310LH	290	28-29	38	310	17-18	2.1	17.5	.39	2.1	<.01	.068	.041	1.35	11.5	.13	.23	.019	.045
330HΦ	290	29-30	11	N/A	N/A	N/A	17.3	.41	1.17	<.01	.042	.013	1.54	23.5	.09	.13	.019	.028
330HL	290	29-30	11	305	17-18	3.1	16.3	.33	1.50	<.01	.052	.082	1.47	18.0	.12	.16	.019	.039
330HM	290	29-30	11	310	17-18	2.7	16.8	.35	1.64	<.01	.079	.010	1.43	18.0	.11	.15	.018	.036
330HH	290	29-30	11	310	17-18	1.7	16.0	.35	1.93	<.01	.014	.048	1.30	12.9	.13	.19	.019	.033
330MM	300	29-30	21	310	18-19	2.7	16.0	.31	1.50	<.01	.079	.075	1.22	14.5	.11	.17	.019	.039
410HΦ	280	29-30	11	N/A	N/A	N/A	15.8	.37	1.20	<.01	.063	.078	.74	5.3	.20	.10	.016	.030
410HL	300	29-30	11	310	18-19	3.1	17.3	.35	1.66	<.01	.100	.072	.90	8.3	.28	.14	.022	.048
410HM	300	29-30	11	310	18-19	2.7	16.0	.32	1.58	<.01	.120	.084	.83	7.0	.24	.12	.021	.042
410HH	300	29-30	11	310	18-19	1.7	17.0	.32	1.62	<.01	.220	.072	.87	7.3	.25	.13	.021	.048
410MH	300	29-30	21	310	18-19	1.7	17.2	.32	1.80	<.01	.071	.076	.96	8.5	.28	.15	.024	.049
410LH	300	29-30	38	310	18-19	1.7	17.9	.33	2.05	<.01	.075	.072	1.15	9.9	.30	.16	.025	.050
312HΦ	320	29-30	11	N/A	N/A	N/A	22.0	.50	1.32	<.01	.070	.066	1.60	10.4	.09	.18	.016	.041
312HH	320	29-30	11	310	18-19	1.7	22.0	.47	1.63	<.01	.079	.058	1.43	10.5	.11	.20	.018	.054
312MM	320	28-29	21	310	18-19	2.7	19.5	.45	1.75	<.01	.100	.050	1.40	10.1	.11	.20	.017	.044
312MH	320	29-30	21	310	18-19	1.7	20.0	.39	1.65	<.01	.080	.076	1.43	10.7	.24	.15	.024	.049

(a) I—current in amperes; V—voltage in volts; S—welding speed in ipm.

determination of 0.999999. The average error resulting from the digitizing and curve fitting is 0.50% as determined from the tungsten standard specimen.

A magnetic inductive type ferrite meter was used to measure the ferrite content of the welds. Calibration of the meter was performed by comparing the magnetic ferrite measurements with point count measurements from two stainless steel weld specimens, one containing 34.2% delta ferrite and the other containing 10.4% delta ferrite, and adjusting the amplifier gain on the meter to read identical with the point count measurements.

During the investigation, it was determined that the ferrite meter required correction when used to measure the ferrite content of the dilatometry specimens. Due to the specimens sharp radius of curvature, the volume-percent ferrite read by the meter was lower than the actual ferrite content. Therefore, the meter was calibrated by measuring the ferrite content of flat specimens and 0.15 in. (3.8 mm) diameter specimens taken from the same weld. The resulting calibration curve, shown in Fig. 2, is presented as a plot of ferrite content measured on the curved surface vs. ferrite content measured on the flat specimen. All ferrite measurements reported in this paper represent an average of at least 10 data points taken on the 0.15 in. (3.8 mm) diameter dilatometry specimen and then converted to the actual ferrite content using the calibration curve of Fig. 2.

Results and Discussion

Thermal Expansion Coefficient and Chemical Composition

A relationship between CTE and chemical composition can be used to predict the thermal expansion properties of dissimilar metal welds by knowing the base metal compositions, filler metal composition and the welding dilution. This relationship was determined by experimentally measuring the CTE of various stainless steel alloys and mapping this data as a function of composition. The DeLong

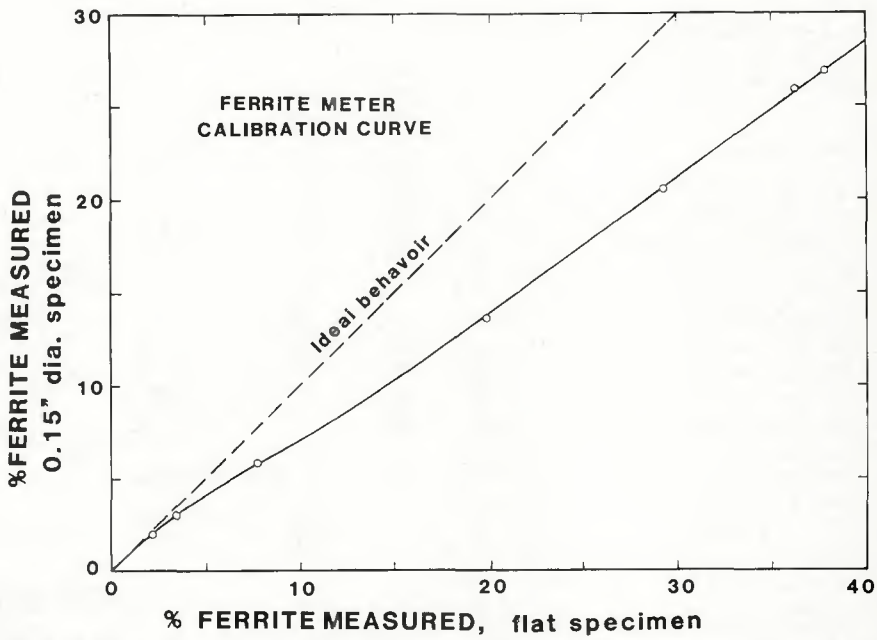

Fig. 2—Ferrite meter calibration curve to correct ferrite measurements made on the curved surface of the dilatometry specimens

Table 2—CTE, Cr_{eq}, Ni_{eq} and Ferrite Content for 28 Stainless Steel Welds

Specimen	Mean Coefficient Thermal Expansion, μm/m/°C, 20 → 400°C	Cr_{eq}	Ni_{eq}	Ferrite, %
308HΦ	18.0	21.3	14.8	10.4
308HL	18.5	21.0	13.9	7.2
308HH	18.4	20.8	14.0	5.6
309HΦ	17.3	24.5	17.1	12.1
309HL	18.2	23.1	17.3	8.1
309HM	18.3	23.6	18.5	5.4
309HH	18.5	22.3	19.4	0.9
309MM	18.9	21.2	17.1	0.5
309LH	18.6	21.1	17.8	0.2
310HΦ	17.7	24.2	20.7	0
310MM	18.3	22.2	16.0	<0.2
310MH	18.1	21.5	17.8	<0.2
310LH	18.7	20.1	15.7	0.9
330HΦ	18.9	19.1	29.6	0
330HL	18.4	18.3	22.9	0
330HM	18.4	19.0	24.3	0
330HH	18.6	18.5	20.3	0
330MM	18.4	18.0	20.0	0
410HΦ	13.9	17.6	10.1	>50[a]
410HL	18.9	19.5	14.1	4.0[a]
410HM	19.0	18.1	13.7	1.4[a]
410HH	19.3	19.1	16.8	1.6[a]
410MH	18.8	19.5	13.8	5.4[a]
410LH	18.7	20.5	15.2	3.6[a]
312HΦ	17.0	24.1	15.6	34.2
312HH	17.5	24.3	15.7	16.9
312MM	18.4	22.2	15.6	4.5
312MH	18.7	21.9	16.5	9.0

(a) Martensite is present.

(Ref. 9), the Schaeffler (Ref. 10) and the Fe-Ni-Cr ternary diagrams were used to map the data as a function of austenite stabilizing elements (i.e., nickel equivalent) and ferrite stabilizing elements (i.e. chromium equivalent). The DeLong method of calculating the Ni equivalent and Cr equivalent:

$$Ni_{eq} = Ni + 0.5\ Mn + 30\ (C + N) \quad (3)$$
$$Cr_{eq} = Cr + Mo + 1.5\ Si \quad (4)$$

was used. These equivalents, as well as the CTE and ferrite contents for the welds, are listed in Table 2.

DeLong Diagram

The majority of the welds have Cr and Ni equivalents that would place them in the compositional limits of the DeLong Constitution Diagram (Ref. 9). Figure 3 shows this diagram with the mean CTE plotted as a function of Cr and Ni equivalents. There are three different regions of interest on this diagram: the single phase austenite field (A), the two phase austenite and ferrite field (A + F), and the three phase austenite, ferrite and martensite field (A + F + M). The CTE is influenced by the presence of these different phases. The highest thermal expansion coefficients were measured in the austenite phase field at a composition of 14 Ni_{eq} and 18 Cr_{eq}, where the CTE is around 19 μm/m/°C. The CTE decreases as the composition is changed in any manner with respect to this point, and the amount that the CTE changes depends on the Cr_{eq} to Ni_{eq} ratio.

If the Cr_{eq} is increased from this region, the composition enters the two phase A + F field. The residual delta ferrite in this region has a BCC crystalline structure and has a lower CTE than austenite. The influence that delta ferrite has on the CTE is discussed in detail in the next section and basically has the effect of reducing the CTE in a predictable manner.

The weld with the highest ferrite content, 312 HΦ with 34.2% ferrite, has the lowest CTE of this region at 17.0 μm/m/°C; this represents a 8.1% reduction in CTE from the austenitic base metal. The same effect in reducing the CTE would be expected if the composition were changed such that the A + F + M region was entered since martensite also has a lower CTE than austenite. One weld containing a significant amount of martensite, 410 HΦ, has a CTE of 13.9 μm/m/°C thereby confirming this trend. This weld, shown in Fig. 4, contains residual delta ferrite outlining the solidification structure in a martensitic matrix and has a hardness of R_c 37.

Each series of filler metal compositions is indicated by a different symbol in Fig. 3 so that the effect of weld dilution on the resulting composition and CTE can be followed. In comparing the CTE data for the welds from the 330 filler metal series and the 410 filler metal series, it is evident that changes in composition that result in formation of phases with thermal expansion properties different from the matrix being present have more effect on changing the CTE than do changes in composition that contribute only solid solution effects. For example, the 330 filler metal is high in nickel content and all the welds are fully austenitic with nickel equivalents in the range of 20 to 24. These welds have similar CTE of about 18.5 μm/m/°C.

Since there are no other phases

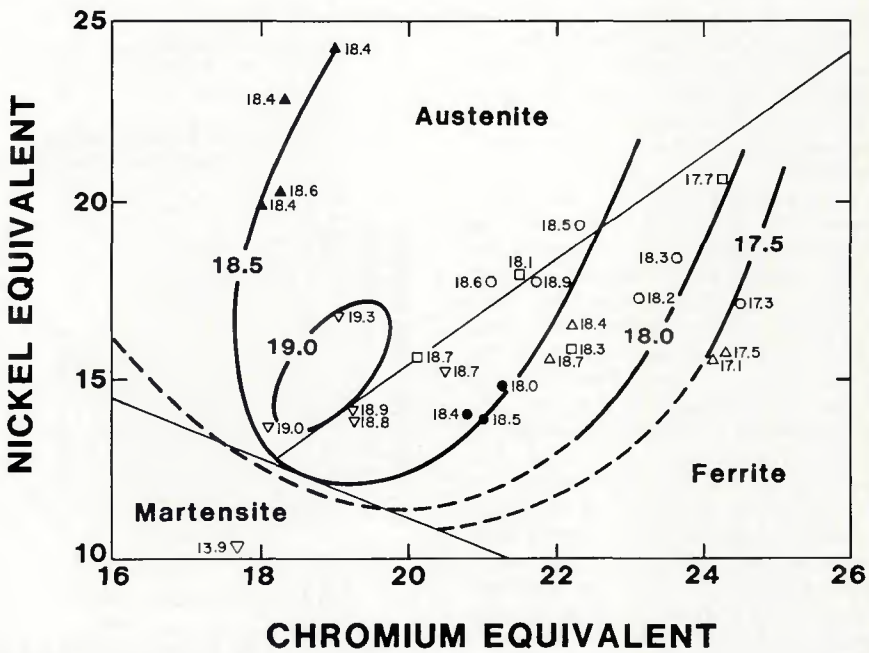

Fig. 3—Mean coefficient thermal expansion (μm/m/°C, 20-400°C, i.e., 68-752°F) plotted on the DeLong diagram as a function of chromium and nickel equivalents. Isoexpansion lines are included. Filler metals: ● 308, O 309, 310, ▲ 312, Δ 330, ▽ 410

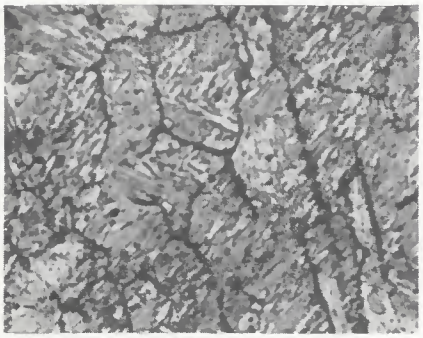

Fig. 4 — Optical micrograph showing martensitic stainless steel weld. Type 410 filler metal; Type 316 base metal; GMA weld. $FeCl_3$ in HNO_3 etchant. X625

present to influence the CTE of fully austenitic welds, there should be a smooth transition in the CTE from 18.5 μm/m/°C to 15.5 μm/m/°C as the nickel content is increased to that of 100% nickel. Therefore, a large increase in nickel content is necessary to reduce the CTE of a fully austenitic alloy by a significant amount.

In contrast, the 410 filler metal series is different in the sense that a small composition variation changes the CTE from 19 μm/m/°C to values as low as 11 μm/m/°C because of the presence of martensite and ferrite in the microstructure. Thus the 410 GMA weld containing ferrite and martensite has a CTE of 13.9 μm/m/°C while the remaining welds in the 410 series, which were heavily diluted with the Type 316 base metal, have CTE values around 19 μm/m/°C.

Fe-Ni-Cr Ternary and Schaeffler Diagram

The narrow compositional range of the DeLong diagram limits its use to stainless steels. Therefore, to obtain an overall understanding of the variation in CTE with composition, CTE data was collected from the literature (Ref. 11-20) pertaining to all Fe-Ni-Cr containing alloys. Similar to the procedure used above with the DeLong diagram, the data were plotted on the ternary diagram and isoexpansion lines were drawn using these data as a guideline. CTE as a function of composition for the Fe-Ni binary system (Ref. 17, 18) and for the Fe-Cr binary system (Ref. 19, 20) was particularly helpful in establishing the contours. Regions where the CTE data exists are shaded. Extrapolation of the contours outside these regions was accomplished by understanding the phases which are present (Ref. 12) and the CTE end points established from work on the binary systems (Ref. 17-20).

The ternary diagram is shown in Fig. 5. The region of highest thermal expansion is again seen in the conventional stainless steel alloys centered about 14 Ni_{eq} and 18 Cr_{eq}. This region represents a peak of CTE at approximately 19 μm/m/°C. Reduction of the Ni_{eq} will result in delta ferrite being present and will decrease the CTE, while a reduction of both the Ni_{eq} and the Cr_{eq} will result in delta ferrite and martensite being present and will also decrease the CTE. The lowest thermal expansion coefficients are observed in the Fe-36Ni, Invar-type, alloys; however, these alloys are not frequently used for welding.

Large variations in the CTE are apparent over the ternary diagram. The most significant changes that occur for ferritic-austenitic stainless steel welds are those that occur due to the presence of delta ferrite and martensite in the microstructure. Therefore, the isoexpansion lines drawn on the ternary diagram were transposed to the conventional Schaeffler Diagram (Ref. 10) so that both the constitution of the weld and its CTE can be predicted from one diagram. This diagram is shown in Fig. 6. The DeLong diagram is outlined to illustrate where the initial data on welds is located, while the shaded areas again represent those regions where CTE data was compiled from the literature. This is a clearer representation of how ferrite and martensite influence the CTE. The martensite causes a trough of low expansion in the diagram while ferrite results in a more gradual decrease in CTE.

The Influence of Delta Ferrite on the CTE

Stainless steel welds will contain residual delta ferrite in the as-welded microstructure if the composition of the weld has a sufficiently high Cr_{eq}/Ni_{eq} ratio. The residual delta ferrite has a BCC crystalline structure, and can be present in various morphologies (Ref. 21) within the FCC austenitic matrix. On solidification, there is a partitioning of ferrite stabilizing elements to the delta ferrite and austenite stabilizing elements to the austenite matrix (Ref. 21). It has already been shown that solid solution effects on the CTE are small and that the important factor in determining the CTE of the material is the CTE of the phases that are present.

To determine the CTE of residual delta ferrite and thus its contribution to the CTE of the duplex structure, a series of dilatometric tests were conducted on a single specimen, 312HΦ, initially containing 34.2% delta ferrite. The residual delta ferrite is metastable and will transform to austenite and sigma phase at elevated temperatures. This phase transformation

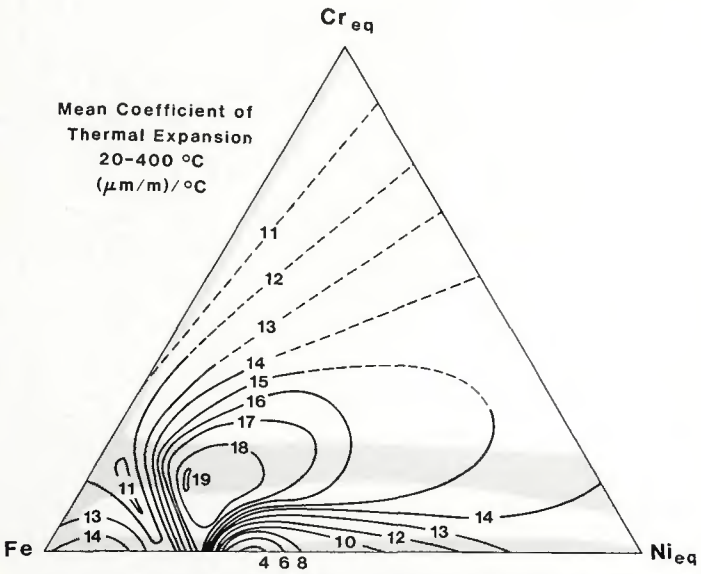

Fig. 5 — Mean coefficient thermal expansion (μm/m/°C, 20-400°C, i.e., 68-752°F) plotted as isoexpansion contours on the Fe-Ni_{eq}-Cr_{eq} ternary diagram. Shaded areas represent regions where data were acquired

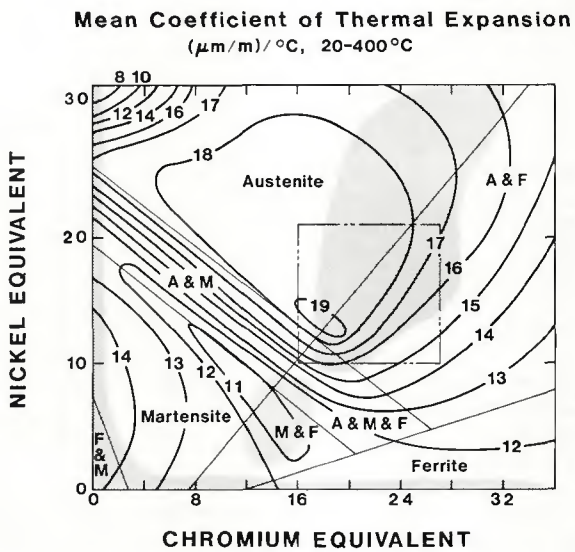

Fig. 6 — Mean coefficient thermal expansion (μm/m/°C, 20-400°C, i.e., 68-752°F) plotted as isoexpansion contours on the Schaeffler constitution diagram. Shaded areas represent regions where data were acquired

Table 3—Ferrite Content, CTE, and Length Measurements After Each of Six Dilatometric Tests Conducted on a High Ferrite Weld

Test no.	Maximum temperature of dilatometric test, °C	Ferrite content after test, vol %	Mean coefficient of thermal expansion, (μm/m)/°C 20 → 400°C	Specimen length: As determined from dilatometric measurements, in.	(mm)	Specimen length: Micrometer measurements, in.	(cm)
As welded	–	34.2	17.2	–		1.5070	(38.278)
1	550	32.7	17.4	1.5068	(38.273)	1.5068	(38.273)
2	650	26.4	17.5	1.5068	(38.273)	1.5062	(38.257)
3	700	18.0	17.8	1.5058	(38.247)	1.5058	(38.247)
4	750	7.0	18.1	1.5050	(38.227)	1.5051	(38.230)
5	800	3.1	18.2	1.5048	(38.222)	1.5049	(38.224)
6	800	2.0	–	1.5047	(38.219)	1.5048	(38.222)

has been studied (Ref. 22-24), and the kinetics of this interface controlled diffusion transformation (Ref. 22) allow it to occur under the thermal cycling conditions of a dilatometric test. Therefore, the specimen was run through several dilatometric cycles that served two purposes:

1. To heat the specimen and transform only part of the ferrite.
2. To measure the CTE of the material, as a function of ferrite content.

A separate metallographic specimen was placed in the dilatometer and subjected to the same thermal cycling as the dilatometric specimen. A section of the metallographic specimen was removed after each thermal cycle to evaluate the microstructure at each ferrite level.

Table 3 summarizes the testing procedures, resulting ferrite contents and CTE of this specimen. The initial dilatometric tests were run at lower maximum temperatures than the latter tests to limit and control the amount of ferrite that transformed. Figure 7 illustrates the CTE as a function of delta ferrite content. As expected, the CTE decreases with increasing ferrite content. The as-welded material containing 34.2% delta ferrite has a CTE of 17.2 μm/m/°C and after five thermal cycles the weld contains 3.1% ferrite and has a CTE of 18.2 μm/m/°C.

Since the residual delta ferrite is distributed as a second phase throughout the austenite matrix, the CTE of the duplex structure may follow a composite theory behavior with delta ferrite content. A review of thermal expansion composite theory relationships by Nielsen (Ref. 25) compares three thermal expansion composite relationships for particulate filled systems. These relationships are the Kerner, Thomas and Turner theories for thermal expansion.

The Thomas equation was selected to represent the expected behavior between the CTE and delta ferrite content because, as Nielsen (Ref. 25) summarizes, the Thomas and the Kerner equations are more accurate in general than the Turner equation and because the Kerner equation requires knowledge of the elastic properties which were not measured in this study. The Thomas theory states:

$$\ln \alpha_c = \Phi_F \ln \alpha_F + \Phi_m \ln \alpha_m \qquad (5)$$

where α is the CTE, Φ is the volume fraction, and the subscripts C, M and F refer to composite, matrix and fiber respectively.

A regression analysis was performed, fitting the data to the mathematical form of the Thomas equation. Extrapolation of this regression line to 0% ferrite predicts the CTE of a fully austenitic material of this composition to be 18.4 μm/m/°C and enables the CTE of ferrite to be calculated from the Thomas equation. The CTE of the residual delta ferrite as determined by this analysis is 15.0 μm/m/°C.

With the CTE of the residual delta ferrite, the Thomas theory can be used to calculate the CTE of a stainless steel weld containing delta ferrite. The CTE of the fully austenitic material can be approximated by the CTE of the stainless steel base metal or filler metal of the same approximate composition in the ferrite free condition, the ferrite content can be measured, and the CTE can be calculated. For example, if an autogeneous weld is made on Type 304L stainless steel base metal resulting in a residual ferrite content of 8%, the CTE of the weld is calculated from equation (5), with the CTE of the austenitic phase taken as the CTE for wrought Type 304 stainless steel material (18.2 μm/m/°C, Ref. 12), to be 17.9 μm/m/°C.

Figure 8 compares the initial and final microstructures of the thermally cycled Type 312 stainless steel weld. Figure 8A shows the as-welded microstructure; the dark etching delta ferrite is present in a continuous vermicular morphology frequently observed in stainless steel welds. After three thermal cycles (Fig. 8B), the ferrite (dark) has transformed to sigma phase (black) and austenite (light). Positive confirmation of the three phases was

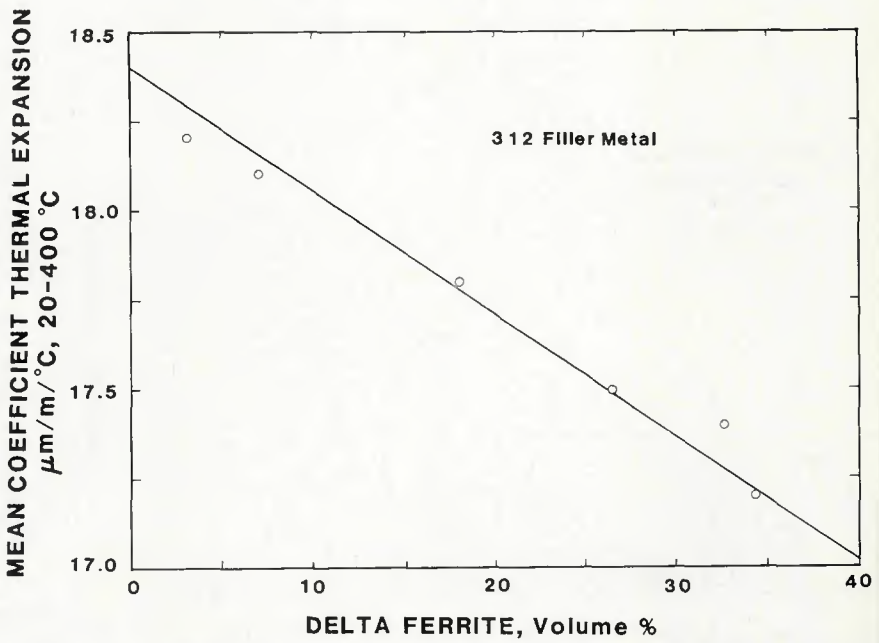

Fig. 7—CTE plotted as a function of residual delta ferrite content illustrating the reduction of CTE with increasing delta ferrite content

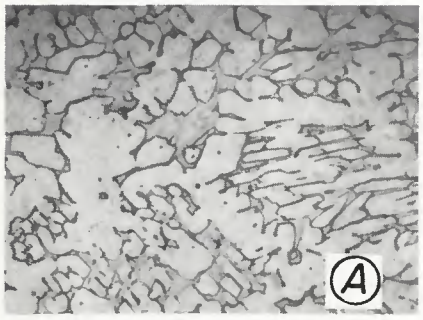

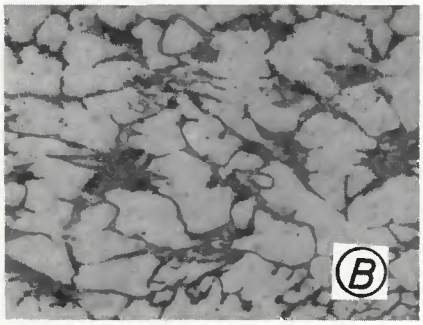

Fig. 8 — Optical micrograph showing the microstructure of Type 312 stainless steel weld in: A — as-welded condition; B — thermally cycled condition. KOH electrolytic etch. X625

accomplished using the magnetic etching technique of Gray, Sikka, and King (Ref. 26) and using Murakamai's etch (Ref. 26); however, a 10% KOH electrolytic etch (1 A/cm^2 for 5 to 7 s) produced the same results and was less time-consuming.

Figure 9 shows the same microstructure at a higher magnification. Figure 9A shows a region of the microstructure where the delta ferrite transformed to sigma phase and austenite in approximately equal amounts; it is to be noted that there appears to be a crystallographic orientation relationship between the newly formed sigma phase and austenite and the original delta ferrite. The transformation of delta ferrite was not uniform throughout the microstructure.

Figure 9B shows a region of the same specimen where much less of the delta ferrite transformed and the sigma phase that is present is not as abundant as that of Fig. 9A. The original ferrite-austenite boundaries are decorated with what seem to be precipitates and they indicate the size of the delta ferrite particle prior to thermal cycling.

After six thermal cycles, a point count of sigma phase shows 14.9% to be present in the microstructure and ferrite measurements show 2.0% ferrite left untransformed. This means that of the initial 34.2% ferrite, only 17.3% of the ferrite in the microstructure transformed directly to austenite.

The presence of sigma phase in the microstructure and its influence on the CTE has not been considered up to this point. However, if the regression line of Fig. 7 is extrapolated to 0% ferrite, with 14.9% sigma phase in the austenitic structure, the material has a CTE of 18.4 μm/m/°C. Comparing this value to that of about 18.5 μm/m/°C for the fully austenitic structures shown in Fig. 3 indicates that there is little difference in the CTE, although one structure contains 14.9% sigma phase and the other is fully austenitic. This leads to the conclusion that sigma phase has a CTE that is nearly the same as that of austenite.

To account for sigma phase, a separate term could be included in equation (3); however, the extra term is not necessary to determine first order effects since the effective CTE of sigma phase in austenite is close to that of the austenitic matrix.

Decrease in Specific Volume as Delta Ferrite Transforms to Austenite

Irreversible dilatometric behavior was observed between heating and cooling cycles of the welded specimens when:

1. The maximum temperature of the test went above about 600°C (1112°F).
2. The weld contained delta ferrite.

In all cases where irreversible behavior was observed, the cooling curve would lie below the heating curve. This type of dilatometric behavior of stainless steel welds has also been observed by Blöch and Huszar (Ref. 24) and is associated with the transformation of delta ferrite. The difference between the heating and cooling curves represents a contraction of the specimen, independent of the thermal expansion (contraction) properties of the material. This behavior is illustrated in Fig. 10, which compares two dilatometric curves of the high ferrite weld series described in the previous section.

Figure 10A shows the typical dilation behavior of the weld when 11.0% of the ferrite transforms. The heating and cooling curves do not superimpose; in fact, the cooling curve lies significantly below the heating curve. There is a negative displacement in the specimen length of 0.0008 in. (0.02 mm), measured at room temperature after the test; this means that the specimen has contracted. In contrast, Fig. 10B shows that the heating and cooling curves almost superimpose when only 1.1% of the ferrite transforms. With subsequent thermal cycling, the material would stabilize and the dilatometric curve would be reversible.

The change in specimen length is due to a decrease in specific volume of the material as the delta ferrite transforms to the more dense austenite and less dense sigma phase. To estimate how much contraction should occur, the densities of Type 410 ferritic stainless steel (7.7 gm/cm^3 — Ref. 13), Type 316 stainless steel (8.0 gm/cm^3 — Ref. 13), and Fe-Cr sigma phase (7.6 gm/cm^3 — Ref. 27) were used to approximate the densities of the phases present in this weld.

With these density approximations, a welded material containing 34.2% ferrite and 65.8% austenite would have a density of 7.90 gm/cm^3, while the same material after thermal cycling containing 2% ferrite, 83.1% austenite and 14.9% sigma phase would have a density of 7.93 gm/cm^3. The difference in specific volume between the material in the as-welded and thermally cycled conditions would be 0.378%.

The relationship, $\Delta V = 3\epsilon_m$, (Ref. 28) where ΔV is the change in specific volume and ϵ_m is the linear strain, is good for small strains and can be used to calculate the strain in any direction to be 1.26×10^{-3} and for the 32.2% change in ferrite, there should be 3.9×10^{-5} strain for each percent ferrite that transforms. Note that this strain would be greater if less sigma phase had been formed as would be the case if a stainless steel base metal less susceptible to forming sigma phase than Type 316 stainless steel would have been used. This value of strain can now be compared to the measured value.

Specimen length as a function of ferrite content is summarized in Table 3 and plotted in Fig. 11. The specimen length at each ferrite level was determined by subtracting the displacement, measured from the dilatometric curve at room temperature, from the previously calculated length. The specimen length was also measured with a micrometer after each test and both measurements are included on this plot.

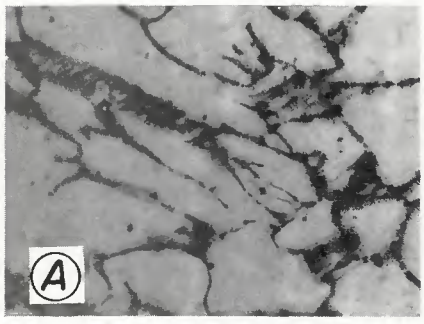

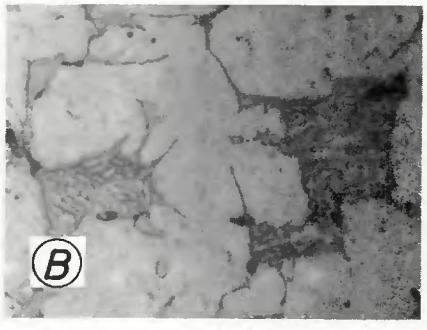

Fig. 9 — Optical micrograph of thermally cycled Type 312 stainless steel weld showing: A — region where delta ferrite transformed to sigma phase and austenite in equal amounts; B — region where very little sigma phase is present upon delta ferrite transformation. KOH electrolytic etch. X1500 (reduced 32% on reproduction)

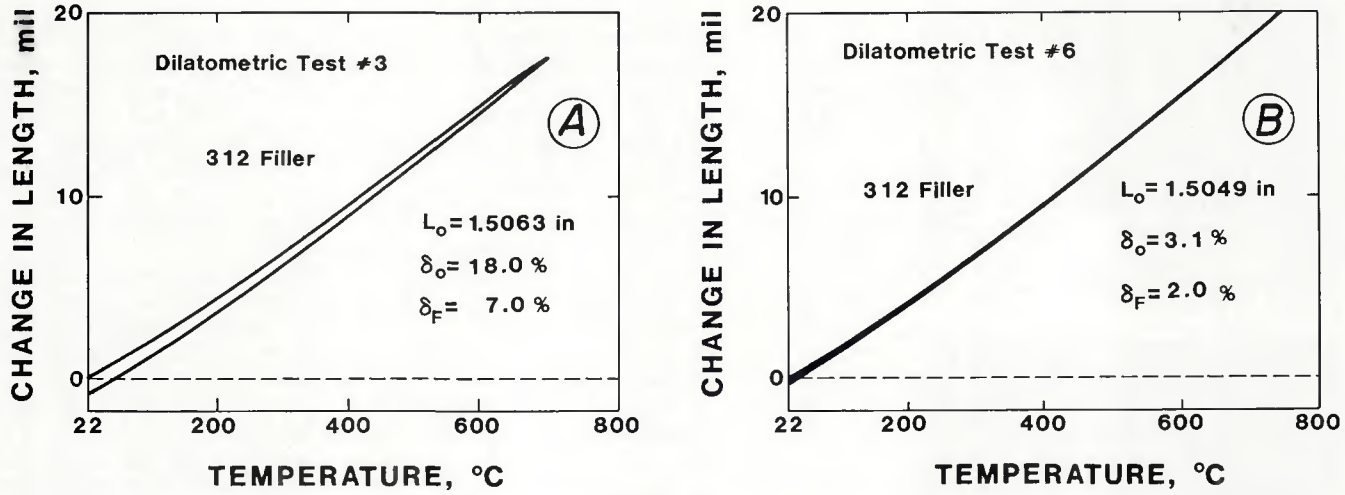

Fig. 10 – Dilatometric curves illustrating a dilation of the specimen as delta ferrite transforms to austenite and sigma phase: A – transformation of 11.0% delta ferrite; B – transformation of 1.1% delta ferrite

The specimen in the as-welded condition was 1.5070 in. (38.278 mm) long, and after six thermal cycles the specimen had contracted to 1.5048 in. (38.222 mm). Thus, the specimen decreased 0.0022 in. (0.056 mm) in length with a 32.2% decrease in ferrite. The change in specimen length with ferrite content can be represented by a linear relationship; this is expected since the volume strain is a direct function of the linear strain for isotropic behavior.

The change in specimen length is the strain which accompanies the phase transformation of delta ferrite to austenite and sigma phase and from this data was calculated to be 4.5×10^{-5} strain for each percent ferrite that transforms. The estimated value for strain, 3.9×10^{-5} for each percent ferrite that transforms, is lower than the measured value but considering the approximations made to obtain the estimated value there is a good correlation. The point to be made, however, is that there is a theoretical basis for the observed contraction.

The implication of a decrease in specific volume during the phase transformation is that, if a stainless steel weld contains delta ferrite and is held at an elevated temperature such that transformation of the ferrite occurs, stresses will develop in the weld joint that will be tensile in nature. These tensile stresses will be over and above the conventional CTE mismatch stresses that are present in the dissimilar metal weld.

CTE mismatch stresses, stress assisted oxidation at the interface, and accelerated creep in a carbon depleted zone close to the weld interface have been cited as problems contributing to the failures of austenitic-ferritic dissimilar metal welds (Ref. 3-6). Stress state at the weld interface is the source of these problems and thus the source of the subsequent cracking that occurs. Thermal expansion mismatch stresses, operating stresses, and static loading stresses contribute to the high stress state at the interface, and the stresses resulting from the phase transformation must also be considered for those welds that contain delta ferrite and are operated at high temperatures. Because the transformation of delta ferrite is an activated process, the stresses that develop from the transformation will do so as a function of time at operating temperatures. Therefore, the stresses in the weld joint may develop over a period of time.

Conclusion

In summary, a means to predict the coefficient of thermal expansion of stainless steel welds has been developed by plotting isoexpansion lines on the DeLong constitution diagram. Twenty-eight data points taken from stainless steel welds provided the means to plot the isoexpansion lines. In addition, the CTE data, supplemented by literature data, was plotted on the Fe-Ni-Cr ternary diagram and on the Schaeffler constitution diagram for weld, wrought and cast materials. Isoexpansion lines were plotted on these diagrams to estimate the CTE as a function of composition; however, these lines can only be considered approximate since the CTE can vary with material processing history. The conclusions from this portion of the study are:

- Changes in composition that result

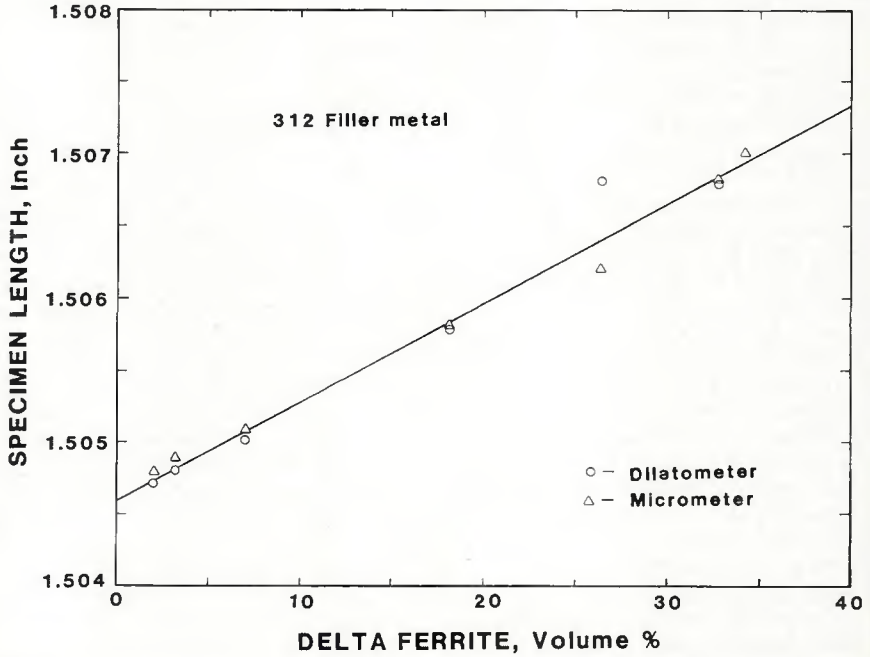

Fig. 11 – Specimen length vs. delta ferrite content showing the contraction of the specimen as delta ferrite transforms to austenite and sigma phase

in martensite or ferrite being present in the microstructure have the largest effect on the CTE of the stainless steel weld.

- Ferrite free stainless steel alloys have the highest CTE of Fe-Ni-Cr ternary alloys. This maximum in CTE occurs at a composition of 14 Ni equivalent, 18 Cr equivalent, and has a value of about 19 μm/m/°C, 20–400°C (68–752°F).
- The CTE is relatively insensitive to changes in composition that occur in the single phase austenite field which contribute only solid solution effects to the CTE.

Ferrite present in a stainless steel weld will reduce its CTE from that in the fully austenitic state. The reduction in CTE corresponds to something less than 10% for typical stainless steel welds. The mean CTE of residual delta ferrite in a duplex structure was calculated to be 15.0 μm/m/°C, 20–400°C (68–752°F), and contributes to the CTE of the duplex structure by the Thomas theory of thermal expansion for composite materials. Using this equation and the CTE of residual ferrite, the CTE of a stainless steel weld can be calculated knowing the delta ferrite content.

A dilation is associated with the transformation of metastable delta ferrite to austenite in ferrite containing stainless steels. This transformation occurs at elevated temperatures as a function of time and corresponds to a decrease in the specific volume of the material. A contractive strain of 4.5×10^{-5} was measured and shown to accompany each per percent ferrite that transforms to austenite and sigma phase. This strain is directly associated with this phase transformation and can have the effect of loading the weld joint in tension.

Acknowledgment

The authors wish to acknowledge the research support of the United States Department of Energy and the assistance of the Republic Steel Corporation. Technical discussions with G. D. Ries of the Republic Steel Corporation and T. A. Whipple of the National Bureau of Standards were helpful and are gratefully appreciated.

References

1. Dalcher, A. W., Yang, T. M., and Chu, C. L. 1977. High temperature thermal-elastic analysis of dissimilar metal transition joints. *Journal of Engineering Materials and Technology* 99 (1):65-69.

2. Bennett, A. P. 1969 (December). Discussion session 5—part A, consumables for fusion welding of dissimilar metals, *Metal Construction* vol. 1: 151.

3. Slaughter, G. M., and Housley, T. R. 1964. The welding of ferritic steels to austenitic stainless steels. *Welding Journal* 43(10): 454-s to 460-s.

4. Blaser, R. U., Eberle, F., and Tucker, J. T., Jr. 1950. Welds between dissimilar alloys in full-size steam piping. *Am. Soc. Testing Mater. Proc.* 50: 789-807.

5. King, J. F., Sullivan, M. D., and Slaughter, G. M. 1977. Development of an improved stainless steel to ferritic steel transition joint. *Welding Journal* 56(11): 345-s to 358-s.

6. Tucker, J. T., and Eberle, F. 1956. Development of a ferritic-austenitic weld joint for steam plant application. *Welding Journal* 35(11): 529-s to 540-s.

7. Kume, R., Okabayashi, H., and Amano, M. 1976 (October). Mechanism of underclad cracking—combined effects of residual strain and heat-affected zone ductility. Transactions of the ASME, *Journal of Materials Engineering and Technology* 98(4): 348-356.

8. Lippold, J. C., and Savage, W. F. 1980. Solidification of austenitic stainless steel weldments: part 2—the effect of alloy composition on ferrite morphology. *Welding Journal* 59(2): 48-s to 58-s.

9. DeLong, W. T., Ostrom, G. A., and Szumachowski, E. R. 1956. Measurement and calculation of ferrite in stainless-steel weld metal. *Welding Journal* 35(11): 521-s to 528-s.

10. Schaeffler, A. L. 1949. Constitution diagram for stainless steel weld metal. *Metals Progress* 56: 680.

11. Touloukian, Y. S., Kirby, R. K., Taylor, R. E., and Desai, P. D. 1975. *Thermophysical Properties of Matter Volume 12 Thermal Expansion,* New York-Washington; IFI, Plenum.

12. Peckner, D., and Bernstein, I. M. 1977. *Handbook of stainless steels,* McGraw Hill.

13. The International Nickel Company, Inc. 1968 (November), *Properties of some metals and alloys.* 3rd ed.

14. Climax Molybdenum Company. 1971. *Thermal expansion data sheets for selected cast high temperature alloys,* Ann Arbor, Michigan.

15. *Material properties handbook volume II, volume IV,* 1966 (May). London W.1: Technical Editing and Reproduction Ltd., Harford House, 7-9 Charlotte St., for the Advisory Group for Aerospace Research and Development.

16. Eldridge, E. A., and Deem, H. W. 1961 (April). *Report on physical properties of metals and alloys from cryogenic to elevated temperatures,* ASTM STP No. 296. American Society for Testing Materials.

17. Wenschhof, D. 1980. *Metals Handbook,* vol. 3, 9th ed.: 792-798. Metals Park, Ohio: American Society for Metals.

18. Marsh, J. S. 1938. *The Alloys of Iron and Nickel, Vol. I Special Purpose Alloys,* Chapter 6, pp. 135-183. McGraw Hill.

19. Touloukian, Y. S., Kirby, R. K., Taylor, R. E., and Desai, P. D. 1975. *Thermophysical properties of matter, volume 12, thermal expansion,* pp. 707-712. New York-Washington: IFI/Plenum.

20. Kinzel, A. B., Franks, R. 1940. *The alloys of iron and chromium, volume II—high chromium alloys,* p. 93. New York and London: McGraw Hill, Inc.

21. David, S. A. 1981. Ferrite morphology and variations in ferrite content in austenitic stainless steel welds. *Welding Journal* 60 (4): 63-s to 73-s.

22. Raghunathan, V. S., Seetharaman, V., Venkadesan, S., and Rodriguez, P. 1979 (November). The influence of post weld heat treatments on the structure, composition and the amount of ferrite in type 316 stainless steel welds. *Metallurgical Transactions A,* 10A: 1683-1689.

23. Wegrzyn, J., and Klimpel, A. 1981. The effect of alloying elements on sigma phase formation in 18-8 weld metals. *Welding Journal* 60(8): 146-s to 154-s.

24. Blöch, R., and Huszar, R. 1980. The disintegration of delta ferrite in welding material X 3 CrNiMoN 25 20. Metallography conference, Augsburg (GFR).

25. Nielsen, L. E. 1967. Mechanical properties of particulate-filled systems. *Journal Composite Materials* 1: 100-119.

26. Gray, R. J., Sikka, V. K., and King, R. T. 1978. Detecting transformation of delta-ferrite to sigma-phase in stainless steels by advanced metallographic techniques. *J. Metals* 30(11): 18-25.

27. Duwez, P., and Baen, S. R. 1950 (June). X-ray study of the sigma phase in various alloy systems. *ASTM STP No. 110:* 48-60.

28. Dieter, G. E. 1976. Mechanical metallurgy, 2nd ed., p. 44. Mcgraw-Hill.